

Transition to dilatation-dominated compressible turbulence

Shadab Alam¹, Christoph Federrath², and Jörg Schumacher^{1*}

¹*Institut für Thermo- und Fluideodynamik, Technische Universität Ilmenau, P.O.Box 100565, D-98684 Ilmenau, Germany*

²*Research School of Astronomy and Astrophysics,*

Australian National University, Canberra, ACT 2611, Australia

(Dated: February 3, 2026)

The kinetic energy dissipation rate is of central importance for the small-scale statistics in turbulent flows. Here, we determine the transition to the dilatation-dominated regime of 3d fully compressible, homogeneous, isotropic turbulence by moments of energy dissipation and its components up to order 4 for turbulent Mach numbers $0.1 \leq M_t \leq 10$. Our high-resolution numerical simulations show a crossover from incompressible to M_t -independent, Burgers turbulence-like moment scaling with respect to Reynolds number Re . This confirms the statistical dominance of shocks for $M_t \gtrsim 1$.

Compressible turbulence introduces additional layers of complexity through mechanisms absent in its incompressible counterpart, including shocklets and shocks, dilatational strain and thermodynamic interactions [1, 2]. These mechanisms shape the flow dynamics in many systems ranging from the interstellar medium (ISM) to engineering applications, such as gas turbines and supersonic propulsion. This is done by modifying the energy cascade [3–8] and thus influencing small-scale statistics and dissipation of kinetic energy [9, 10]. The turbulent Mach number $M_t = u_{\text{rms}}/c_s$ and the large-scale Reynolds number $Re = u_{\text{rms}}L_f/\nu$ characterize, respectively, the level of compressibility and the vigor of turbulence, where ν is the kinematic viscosity, L_f is the forcing length scale, c_s is the speed of sound, $u_{\text{rms}} = \sqrt{\langle \mathbf{u}^2 \rangle_{V,t}}$ is the root-mean-square of the velocity field \mathbf{u} , and $\langle \cdot \rangle_{V,t}$ denotes the average over volume V and time t .

A defining characteristic of fully turbulent flows is spatial intermittency—the emergence of strongly localized bursts, steep fronts and intense vortices at the small-scale end of the inertial cascade close to the Kolmogorov dissipation length η [11–16]. They give rise to strongly non-Gaussian statistics of turbulence fields and their derivatives, in particular the kinetic energy dissipation rate ϵ , which is given by

$$\epsilon(\mathbf{x}, t) = 2\mu \mathbf{S} : \mathbf{S} - \frac{2\mu}{3}(\nabla \cdot \mathbf{u})^2, \quad (1)$$

with the dynamic viscosity $\mu = \rho\nu$ and the rate-of-strain tensor $\mathbf{S} = [\nabla \mathbf{u} + (\nabla \mathbf{u})^T]/2$, which probes the strength of local shear. In the inertial range for scales $\ell > \eta$ and at $M_t \leq 1$, the structure functions of the velocity field were found to follow scaling laws close to incompressible predictions [17, 18]. In Lagrangian studies of compressible turbulence, the situation is slightly different. For $M_t \lesssim 0.5$, the statistics remain essentially incompressible [19, 20]; however, deviations become evident at higher M_t [20, 21] as shocklets begin to influence the dynamics. Supersonic isothermal simulations at $M_t = 6$ and 17 [6, 22] exhibited for example kinetic energy spec-

tra close to the shock-dominated Burgers turbulence-type k^{-2} scaling, together with larger values of the low-order structure-function exponents [22] compared to incompressible turbulence. The deviations increase when the volume forcing of the compressible flow injects additional velocity field divergence into the flow [6, 21, 23], i.e., when it becomes increasingly dilatational. These results clearly reflect the growing impact of shocks on the turbulence statistics.

As we have seen, most analysis of compressible turbulence focused on the statistics in the inertial cascade range, such as scaling laws for energy spectra and structure functions at sufficiently high Reynolds numbers. Here, we will turn the attention from the velocity to the velocity derivative statistics at somewhat smaller Reynolds numbers. In these cases, an inertial cascade range is absent, but we will show that the intermittent statistical properties of derivatives have already developed, e.g., for the kinetic energy dissipation rate and, in compressible flow case, its solenoidal and dilatational components. It is known from incompressible flows that derivative moments transition from Gaussian to intermittent scaling at $Re \sim 10^2$ [24–31]. The same holds for Burgers turbulence [32]. These scalings of velocity structure functions and moments of velocity derivatives can then be connected by fusion rules, which in case of the energy dissipation moments in incompressible turbulence leads to

$$M_n = \frac{\langle \epsilon^n \rangle_{V,t}}{\langle \epsilon \rangle_{V,t}^n} \propto Re^{\beta_n} \quad \text{with} \quad \beta_n = n + \frac{\zeta_{4n}}{\zeta_{4n} - \zeta_{4n+1} - 1}.$$

The scaling exponents β_n depend nonlinearly on the order n (via the structure function exponents ζ_n), thus reflecting the intermittent character of the fields by an anomalous moment scaling with respect to Re [24].

Here, we conduct a series of direct numerical simulations (DNS) of compressible turbulence at very high resolution. We monitor the Reynolds number scaling of $M_n(Re)$ for different degrees of compressibility, quanti-

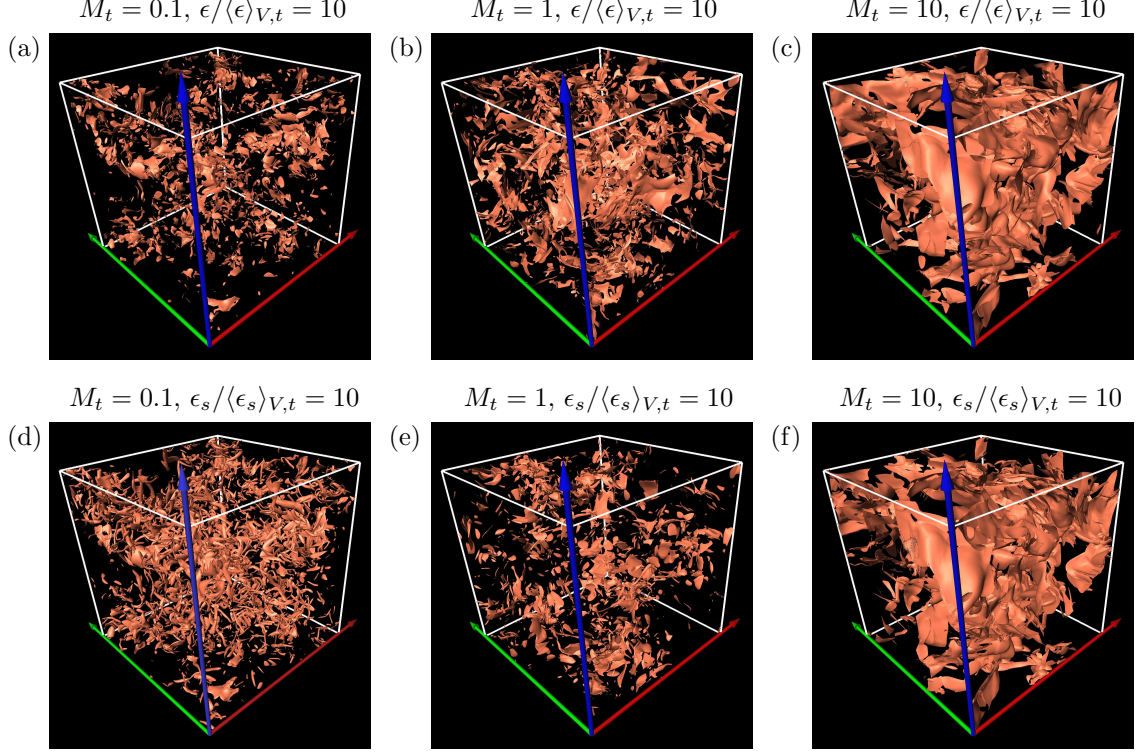


FIG. 1. Structure of the kinetic energy dissipation rate field. Isosurface snapshots of total energy dissipation $\epsilon(\mathbf{x}, t_0)$ at the level $\epsilon = 10\langle\epsilon\rangle_{V,t}$ (top row) and its solenoidal component $\epsilon_s(\mathbf{x}, t_0)$ at $\epsilon_s = 10\langle\epsilon_s\rangle_{V,t}$ (bottom row) for turbulent Mach numbers $M_t = 0.1$ (a, d), $M_t = 1$ (b, e) and $M_t = 10$ (c, f). All data are obtained at the highest Reynolds number $Re \approx 2400$; isosurfaces are displayed for the decadic logarithm of the fields.

fied by the turbulent Mach number M_t . Our main finding is a detection of a transition from a solenoidal statistics of moments M_n for $M_t \lesssim 1$ to a close-to-Burgers-turbulence-type behavior for $M_t > 1$, where the energy dissipation is dominated by its dilatational dynamics.

Simulations. The high-resolution DNS of three-dimensional homogeneous, isotropic, compressible turbulence solve the following equations,

$$\frac{\partial \rho}{\partial t} + \nabla \cdot (\rho \mathbf{u}) = 0, \quad (2)$$

$$\frac{\partial(\rho \mathbf{u})}{\partial t} + \nabla \cdot (\rho \mathbf{u} \otimes \mathbf{u}) = -\nabla p + \nabla \cdot \boldsymbol{\sigma} + \rho \mathbf{f}, \quad (3)$$

together with the isothermal equation of state, $p = \rho c_s^2$. Here, ρ is the mass density, p the pressure, $\boldsymbol{\sigma}$ the viscous stress tensor, and \otimes denotes the dyadic product. The flow is driven by a stochastic forcing \mathbf{f} implemented in Fourier space using an Ornstein–Uhlenbeck (OU) process [33, 34]. The forcing is *purely solenoidal*, applied at the smallest wavenumbers, $1 < k L/2\pi < 3$, with a parabolic spectral distribution peaking at $k L/2\pi = 2$, where L is the domain size. This corresponds to a characteristic forcing length scale $L_f \approx L/2$. The equations are solved in a triply periodic cube of volume $V = L^3$ using a modified version of the FLASH code [2, 35, 36].

Our DNS cover turbulent Mach numbers $0.1 \leq M_t \leq$

10, spanning subsonic and supersonic regimes (see Supplementary Material for details on the DNS parameters and the numerical method). In summary, all DNS are performed at high spatial resolutions with $k_{\max} \eta \geq 11$, where $k_{\max} = \pi N/L$ and the Kolmogorov length scale $\eta = (\langle \rho \rangle_{V,t} \nu^3 / \langle \epsilon \rangle_{V,t})^{1/4}$. We conducted 56 simulations on uniform meshes with up to $N^3 = 2048^3$ grid points. The attainable Reynolds numbers are $100 \lesssim Re \lesssim 2400$ [37], with corresponding Taylor microscale Reynolds numbers $15 \lesssim Re_\lambda = \sqrt{(5\langle \rho \rangle_{V,t} / (3\nu \langle \epsilon \rangle_{V,t}) u_{\text{rms}}^2)} \lesssim 117$. All DNS thus start beyond the transition from Gaussian to non-Gaussian statistics [38]. For each simulation, a number of N_s snapshots of the statistically stationary state are taken at intervals of one quarter of the large-scale eddy turnover time L_f/u_{rms} for statistical analysis.

Similar to the Helmholtz decomposition of the velocity field into solenoidal and dilatational parts, $\mathbf{u} = \mathbf{u}_s + \mathbf{u}_d$, with $\nabla \cdot \mathbf{u}_s = 0$, and $\nabla \times \mathbf{u}_d = 0$, we can decompose the kinetic energy dissipation rate field (1) into solenoidal, dilatational, and inhomogeneous components [39–41],

$$\epsilon = \epsilon_s + \epsilon_d + \epsilon_I, \quad (4)$$

with (see Supplementary Material for details)

$$\epsilon_s(\mathbf{x}, t) = \mu(\nabla \times \mathbf{u})^2, \quad \epsilon_d(\mathbf{x}, t) = \frac{4}{3}\mu(\nabla \cdot \mathbf{u})^2,$$

$$\epsilon_I(\mathbf{x}, t) = 2\mu [(\nabla \otimes \nabla) : (\mathbf{u} \otimes \mathbf{u}) - 2\nabla \cdot (\mathbf{u}(\nabla \cdot \mathbf{u}))].$$

Figure 1 (a–c) displays isosurfaces at $\epsilon = 10\langle\epsilon\rangle_{V,t}$ of the simulations with $M_t = 0.1, 1$ and 10 and the highest Re . We see that $\epsilon(\mathbf{x}, t)$ crosses over from local shear layers (panel a), caused by the self-induced strain due to vortex stretching [42], to extended, stacked shock-generated sheets (panel c) for the highly supersonic case. Figure 1 (d–f) displays isosurfaces of $\epsilon_s = 10\langle\epsilon_s\rangle_{V,t}$ at $M_t = 0.1, 1$ and 10 and the highest Reynolds number, in addition to the total dissipation ϵ in the top row. We see that the solenoidal part ϵ_s changes from tube-like patterns in panel (d), which are typical for the local enstrophy in the incompressible case [12], to almost identical shock-surface patterns, similar to the total dissipation ϵ at $M_t = 10$, cf. panels (c) and (f). We now investigate how these structures manifest in the small-scale statistical properties.

Points in the M_t – δ plane and mean dissipation. We first determine the operating points of our DNS runs in the parameter space of compressible turbulence. In addition to the two central parameters, Re and M_t , a third relevant one is the dilatational parameter (see e.g. [43]),

$$\delta = \frac{u_{d,\text{rms}}}{u_{s,\text{rms}}}, \quad (5)$$

which quantifies the ratio of dilatational to solenoidal motions in compressible flow. Figure 2(a) shows our DNS series with solenoidal forcing in the δ – M_t plane. We see an asymptotic behavior for the supersonic DNS to approximately $\delta \simeq 0.5$. This finding is consistent with an earlier study [44], which yielded an asymptotic ratio of $E_{\text{sol}}/E_{\text{tot}} = u_{s,\text{rms}}^2/(u_{s,\text{rms}}^2 + u_{d,\text{rms}}^2) \simeq 0.8 \Rightarrow \delta \simeq 1/2$ for purely solenoidal forcing in the limit $M_t \rightarrow \infty$. Furthermore, it is consistent with a renormalization group analysis, which gave a ratio $u_{s,\text{rms}}^2/u_{d,\text{rms}}^2 = 3$, corresponding to $\delta = 1/\sqrt{3} \approx 0.58$ [45].

We show the ratios of $\langle\epsilon_d\rangle_{V,t}/\langle\epsilon\rangle_{V,t}$ and $\langle\epsilon_d\rangle_{V,t}/\langle\epsilon_s\rangle_{V,t}$ versus M_t in Fig. 2 (b,c). Panel (b) shows that the dilatational fraction of dissipation is rising from almost zero to $\simeq 0.5$, underlining the increasing role of compressive motions and shock-driven dissipation with increasing Mach number. At the highest Mach number, $M_t = 10$, the dilatational-to-solenoidal mean dissipation ratio (panel c) is $\lesssim 1$. We have seen that the isosurfaces of ϵ_s at this Mach number also form sharp, sheet-like patterns aligned with shocks, likely indicating vorticity amplification in shock–turbulence interactions; this enhanced vorticity increases solenoidal dissipation and may contribute to the observed magnitude of the ratio of about unity for $M_t > 1$. In the subsonic regime for $0.3 \leq M_t \leq 1$, the ratio follows an approximate M_t^5 scaling, which is consistent with ref. [46]; a similar but slightly shallower $M_t^{4.1}$ scaling was reported in [47].

The rate-of-strain tensor can also be Helmholtz-decomposed into two parts, $\mathbf{S} = \mathbf{S}_s + \mathbf{S}_d$ with $\mathbf{S}_s = [\nabla \mathbf{u}_s + (\nabla \mathbf{u}_s)^T]/2$ and $\mathbf{S}_d = [\nabla \mathbf{u}_d + (\nabla \mathbf{u}_d)^T]/2$. Thus

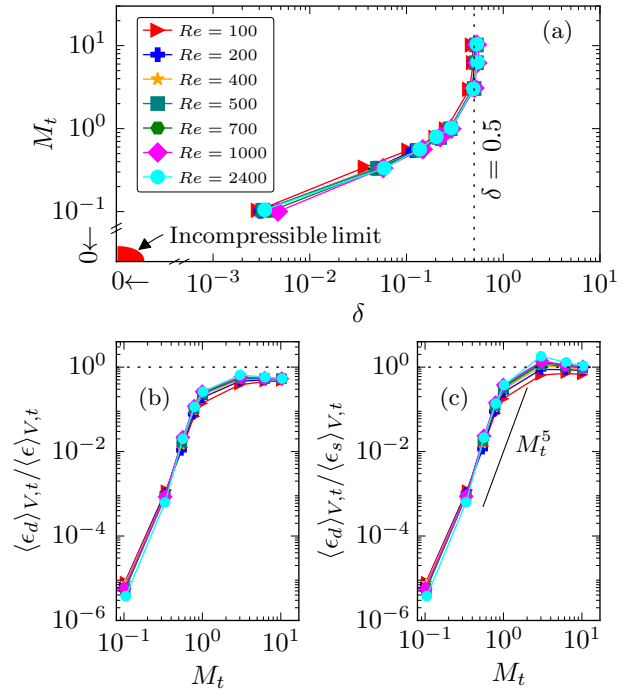


FIG. 2. (a) Operating points of the solenoidally forced compressible turbulence simulations in the δ – M_t parameter plane (panel a). The incompressible limit and the δ -asymptote are indicated, which is consistently not exceeded by our simulations. Panels b and c show the ratios of the mean dissipation rates versus the turbulent Mach number M_t : (b) $\langle\epsilon_d\rangle_{V,t}/\langle\epsilon\rangle_{V,t}$ and (c) $\langle\epsilon_d\rangle_{V,t}/\langle\epsilon_s\rangle_{V,t}$. The dotted horizontal lines indicate asymptotic behavior toward a 1:1 ratio.

(1) can be rewritten as

$$\epsilon(\mathbf{x}, t) = 2\mu(\mathbf{S}_s : \mathbf{S}_s + \mathbf{S}_d : \mathbf{S}_d + 2\mathbf{S}_s : \mathbf{S}_d) - \frac{2\mu}{3}(\nabla \cdot \mathbf{u}_d)^2. \quad (6)$$

The first summand in the first term is denoted as $\epsilon_{\text{inc}} = 2\mu\mathbf{S}_s : \mathbf{S}_s$, the pointwise dissipation rate arising from the incompressible motion in the flow. Consequently, ϵ can be written as $\epsilon = \epsilon_{\text{inc}} + \epsilon_{\text{com}}$, i.e., as the sum of the incompressible and compressible dissipation fields (which consists of the remaining terms in (6)). This is an alternative decomposition in comparison to (4), motivated by the original expression for the incompressible energy dissipation field. We find that the mean values $\langle\epsilon_{\text{inc}}\rangle_{V,t}$ and $\langle\epsilon_{\text{com}}\rangle_{V,t}$ behave similarly to $\langle\epsilon_s\rangle_{V,t}$ and $\langle\epsilon_d\rangle_{V,t}$ in Fig. 2, respectively (not shown). Although ϵ_{inc} and ϵ_s both arise from solenoidal motions, they are conceptually distinct in their local structure: the former is associated with local shear layers, whereas the latter with the vortical structures in the fluid. We will investigate both dissipation field components in their Re -scaling, which turns out to be slightly different.

Scaling of dissipation moments. We summarize the scaling exponents $\beta_{k,n}$ versus M_t for the energy dissipation moments $M_{k,n}(Re)$ of orders $n = 2, 3$ and 4 in

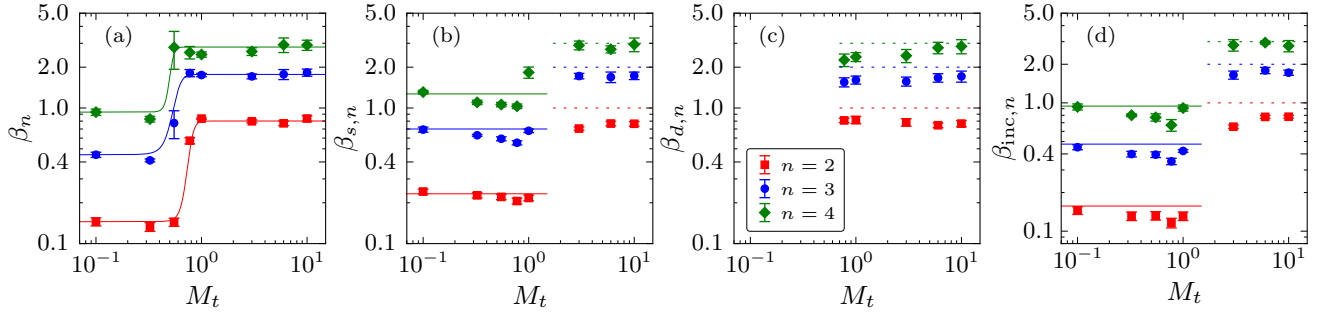


FIG. 3. Reynolds number-scaling exponents of the 2nd-, 3rd- and 4th-order moments of the total dissipation rate (a), solenoidal component (b), dilatational component (c), and incompressible component (d), as functions of the turbulent Mach numbers M_t . In the incompressible limit $M_t \ll 1$, $\beta_{\text{inc},n} = \beta_n$ and are consistent with those reported for incompressible isotropic turbulence [24, 26, 48]; $\beta_2 = 0.157$, $\beta_3 = 0.489$ and $\beta_4 = 0.944$. In this limit, the solenoidal exponents (b) take the values $\beta_{s,2} = 0.242$, $\beta_{s,3} = 0.693$, and $\beta_{s,4} = 1.31$, in close agreement with Elsinga *et al.* [49] after necessary adjustment, see Supplementary Material. For $M_t > 1$, the exponents are very close to the Burgers' scaling exponents. In panel (a), the data points are connected by a tanh fitting curve. The solid and dotted reference lines indicate the scaling exponents of incompressible and Burgers turbulence limits, respectively.

Fig. 3. Here, $k = \{s, d, \text{inc}\}$ in panels (b–d); panel (a) shows the total dissipation for completeness. In the low-Mach number regime for $M_t \leq 0.33$, the total dissipation exponents β_n in panel (a) align well with predictions from incompressible turbulence theory [24, 48] and DNS study [26, 28]. The data points are connected by fitting curves in panel (a), which correspond to the incompressible exponents for $M_t \ll 1$.

For $M_t \geq 0.55$, the scaling exponents of all moments rise significantly and saturate to a plateau in the supersonic cases for $M_t > 1$. In particular, the DNS runs at $M_t = 0.55$ are characterized by high-amplitude events of $M_{k,n}$ in the time sequence of snapshots that dominate the statistics of the whole data set. In the Supplementary Material we provide $\min(M_4)$ and $\max(M_4)$ of ϵ for the whole sequence of N_s snapshots and show the statistical convergence of the 4th-order total dissipation moments M_4 for all Mach numbers and $Re = 2400$ (Suppl. Fig. 1). We interpret these as critical fluctuations of the transition to dilatation-dominated compressible turbulence. This process manifests in the form of first evolving dominant pre-shocks, which mature to an increasing number of shocks for $M_t \gtrsim 1$, see panels (a) and (c) of Fig. 3. In contrast, the solenoidal and incompressible exponents (panels b and d), remain relatively unchanged for $M_t \leq 1$, with solenoidal values exceeding incompressible ones—consistent with findings that ϵ_s is more intermittent than ϵ_{inc} for $Re_\lambda \lesssim 400$ [50, 51]. Moreover, the exponents of the dilatational dissipation moments, $\beta_{d,n}$ (panel c) are almost constant with comparable values for $M_t > 0.55$, pointing anew to an increasing contribution from shock and pre-shock structures.

What determines the plateau limit for the β 's in all panels? In one-dimensional, stochastically forced Burgers turbulence, it was shown by Friedrich *et al.* [32] that

the normalized moments of the derivative $\partial_x u$ satisfy an anomalous scaling relation for $Re \gg 1$, which can be translated into a scaling of dissipation rate moments as follows,

$$\tilde{M}_n = \frac{\langle (\partial_x u)^n \rangle}{\langle (\partial_x u)^2 \rangle^{n/2}} \sim Re^{n/2-1} \Rightarrow M_n \sim Re^{n-1}, \quad (7)$$

using $\epsilon \sim (\partial_x u)^2$. If we now inspect the values of the plateaus of $\beta_{k,n}$ in Fig. 3, we see that they fall consistently below 1, 2, and 3 for M_2 , M_3 , and M_4 , respectively. This clearly supports the physical picture that the anomalous exponents of shock-dominated Burgers turbulence (with pressure being absent) bound those of fully compressible turbulence from above.

Finally, we study how important the fluctuations of the density are, which enter the energy dissipation via the dynamic viscosity μ . To this end, we analyze the scaling of $M_n^\rho = \langle \rho^n \rangle / \langle \rho \rangle^n \sim Re^{\beta_n^\rho}$. For $M_t < 1$, all exponents $\beta_n^\rho = 0$. For $M_t > 1$, an anomalous scaling of the density moments is observed in Fig. 4, a further footprint of the transition to dilatation-dominated turbulence. The spatial intermittency of the density field is visible in the inset at $M_t = 10$, where ρ is characterized by sharp fronts of high density between relatively homogeneous regions. This spatial intermittency additionally amplifies the Burgers-type statistics of ϵ and its components.

Conclusion. Our numerical simulations of compressible turbulence report a transition of the velocity derivative statistics, here in the form of scaling laws for the kinetic energy dissipation and its components with Re , from the scaling for the low-Mach number limit ($M_t \ll 1$) to a Burgers turbulence-type scaling for $M_t \gg 1$, the latter of which is dominated by shock structures and dilatation effects for the density and energy dissipation fields.

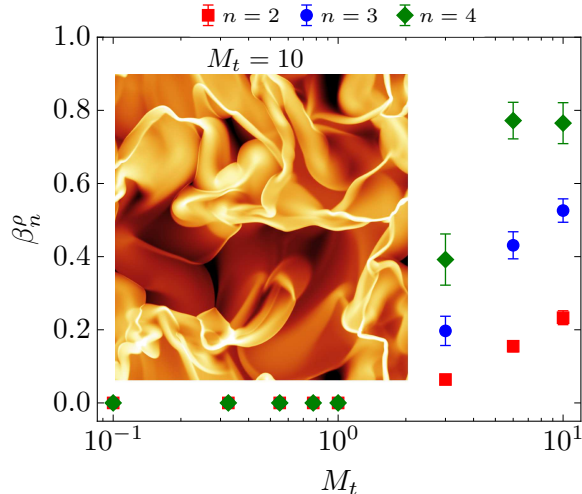


FIG. 4. Scaling exponents β_n^ρ of the density moments M_n^ρ versus M_t . The inset shows a density contour plot in a two-dimensional plane at $M_t = 10$ and $Re = 2400$, plotted as $\log_{10}(\rho/\langle \rho \rangle_{V,t}) \in (-3, 1)$.

This transition is relatively sharp for all moment orders at $M_t \sim 1$. Both components of dissipation, ϵ_s and ϵ_d , scale similarly for $M_t > 1$. The intermittency of the dissipation field is amplified in addition by an intermittency of the density in the supersonic cases. It remains to be seen if this relatively sharp transition stays intact when the forcing of the turbulence includes dilatational components, even at $M_t < 1$.

Acknowledgements

S.A. and J.S. are supported by the European Union (ERC, MesoComp, 101052786). Views and opinions expressed however are those of the authors only and do not necessarily reflect those of the European Union or the European Research Council. S.A. was also partly supported by grant no. SCHU 1410/31-1 of the Deutsche Forschungsgemeinschaft. C.F. acknowledges funding provided by the Australian Research Council (Discovery Projects DP230102280 and DP250101526), and the Australia-Germany Joint Research Cooperation Scheme (UA-DAAD). The authors acknowledge the Gauss Centre for Supercomputing (GCS) e.V. (<https://www.gauss-centre.eu>) for funding this work by providing computing time on the GCS Supercomputer SuperMUC-NG at the Leibniz Supercomputing Centre (<https://www.lrz.de>) within the compute projects pn68ni, pn67la, pr32lo, and pr48pi. We further acknowledge GCS Large-scale project 10391, the Australian National Computational Infrastructure (grant ek9) and the Pawsey Supercomputing Centre (project pawsey0810) in the framework of the National Computational Merit Allocation Scheme and the ANU Merit Allocation Scheme.

* joerg.schumacher@tu-ilmenau.de

- [1] D. A. Donzis and S. Jagannathan, Fluctuations of thermodynamic variables in stationary compressible turbulence, *J. Fluid Mech.* **733**, 221 (2013).
- [2] C. Federrath and S. Offner, Computational advances and challenges in simulations of turbulence and star formation, *Living Rev. Comput. Astrophys.* , arXiv:2510.12203 (2025).
- [3] H. Aluie, Compressible turbulence: the cascade and its locality, *Phys. Rev. Lett.* **106**, 174502 (2011).
- [4] S. Galtier and S. Banerjee, Exact relation for correlation functions in compressible isothermal turbulence, *Phys. Rev. Lett.* **107**, 134501 (2011).
- [5] J. Wang, Y. Yang, Y. Shi, Z. Xiao, X. He, and S. Chen, Cascade of kinetic energy in three-dimensional compressible turbulence, *Phys. Rev. Lett.* **110**, 214505 (2013).
- [6] C. Federrath, On the universality of supersonic turbulence, *Mon. Not. R. Astron. Soc.* **436**, 1245 (2013).
- [7] A. G. Krtsuk, R. Wagner, and M. L. Norman, Energy cascade and scaling in supersonic isothermal turbulence, *J. Fluid Mech.* **729**, R1 (2013).
- [8] G. L. Eyink and T. Drivas, Cascades and Dissipative Anomalies in Compressible Fluid Turbulence, *Phys. Rev. X* **8**, 011022 (2018).
- [9] L. Pan, P. Padoan, and A. G. Krtsuk, Dissipative structures in supersonic turbulence, *Phys. Rev. Lett.* **102** (2009).
- [10] J. Panickacheril John, D. A. Donzis, and K. R. Sreenivasan, Does dissipative anomaly hold for compressible turbulence?, *J. Fluid. Mech.* **920**, A20 (2021).
- [11] Z.-S. She, E. Jackson, and S. A. Orszag, Intermittent vortex structures in homogeneous isotropic turbulence, *Nature* **344**, 226 (1991).
- [12] J. Schumacher, B. Eckhardt, and C. R. Doering, Extreme vorticity growth in Navier-Stokes turbulence, *Phys. Lett. A* **374**, 861 (2010).
- [13] K. Iyer, J. Schumacher, K. R. Sreenivasan, and P. K. Yeung, Steep cliffs and saturated exponents in three-dimensional turbulence, *Phys. Rev. Lett.* **121**, 264501 (2018).
- [14] D. Buarria, A. Pumir, E. Bodenschatz, and P. K. Yeung, Extreme velocity gradients in turbulent flows, *New J. Phys.* **21**, 043004 (2019).
- [15] D. Buarria, J. M. Lawson, and M. Wilczek, Extreme velocity gradients in turbulent flows, *Sci. Adv.* **10**, eado1969 (2024).
- [16] K. R. Sreenivasan and J. Schumacher, What is the turbulence problem, and when may we regard it as solved?, *Annu. Rev. Condens. Matter Phys.* **15**, 121 (2025).
- [17] J. Wang, Y. Shi, L.-P. Wang, Z. Xiao, X. T. He, and S. Chen, Scaling and statistics in three-dimensional compressible turbulence, *Phys. Rev. Lett.* **108**, 214505 (2012).
- [18] J. Wang, T. Gotoh, and T. Watanabe, Scaling and intermittency in compressible isotropic turbulence, *Phys. Rev. Fluids* **2**, 053401 (2017).
- [19] R. Benzi, L. Biferale, R. Fisher, D. Q. Lamb, and F. Toschi, Inertial range Eulerian and Lagrangian statistics

tics from numerical simulations of isotropic turbulence, *J. Fluid Mech.* **653**, 221–244 (2010).

[20] Y. Yang, J. Wang, Y. Shi, Z. Xiao, X. T. He, and S. Chen, Intermittency caused by compressibility: a Lagrangian study, *J. Fluid Mech.* **786**, R6 (2016).

[21] L. Konstandin, C. Federrath, R. S. Klessen, and W. Schmidt, Statistical properties of supersonic turbulence in the Lagrangian and Eulerian frameworks, *J. Fluid Mech.* **692**, 183 (2012).

[22] A. G. Kritsuk, M. L. Norman, P. Padoan, and R. Wagner, The statistics of supersonic isothermal turbulence, *Astroph. J.* **665**, 416 (2007).

[23] W. Schmidt, C. Federrath, and R. Klessen, Is the scaling of supersonic turbulence universal?, *Phys. Rev. Lett.* **101**, 194505 (2008).

[24] V. Yakhot, Probability densities in strong turbulence, *Physica D* **215**, 166 (2006).

[25] J. Schumacher, Sub-Kolmogorov-scale fluctuations in fluid turbulence, *Europhys. Lett.* **80**, 54001 (2007).

[26] J. Schumacher, K. R. Sreenivasan, and V. Yakhot, Asymptotic exponents from low-Reynolds-number flows, *New. J. Phys.* **9**, 89 (2007).

[27] J. Schumacher, J. D. Scheel, D. Krasnov, D. A. Donzis, V. Yakhot, and K. R. Sreenivasan, Small-scale universality in fluid turbulence, *Proc. Natl. Acad. Sci.* **111**, 10961 (2014).

[28] V. Yakhot and D. A. Donzis, Emergence of multiscaling in a random-force stirred fluid, *Phys. Rev. Lett.* **119**, 044501 (2017).

[29] J. Schumacher, A. Pandey, V. Yakhot, and K. R. Sreenivasan, Transition to turbulence scaling in Rayleigh–Bénard convection, *Phys. Rev. E* **98**, 033120 (2018).

[30] K. R. Sreenivasan and V. Yakhot, Dynamics of three-dimensional turbulence from Navier–Stokes equations, *Phys. Rev. Fluids* **6**, 104604 (2021).

[31] T. Gotoh and J. Yang, Transition of fluctuations from Gaussian state to turbulent state, *Phil. Trans. R. Soc. A* **380**, 20210097 (2022).

[32] J. Friedrich, G. Margazoglou, L. Biferale, and R. Grauer, Multiscale velocity correlations in turbulence and Burgers turbulence: Fusion rules, Markov processes in scale, and multifractal predictions, *Phys. Rev. E* **98**, 023104 (2018).

[33] C. Federrath, J. Roman-Duval, R. S. Klessen, W. Schmidt, and M. Mac Low, Comparing the statistics of interstellar turbulence in simulations and observations. Solenoidal versus compressive turbulence forcing, *A&A* **512**, A81 (2010).

[34] C. Federrath, J. Roman-Duval, R. S. Klessen, W. Schmidt, and M. M. Mac Low, TG: Turbulence Generator, *Astrophysics Source Code Library*, record ascl:2204.001 (2022), ascl:2204.001.

[35] B. Fryxell, K. Olson, P. Ricker, F. X. Timmes, M. Zingale, D. Q. Lamb, P. MacNeice, R. Rosner, J. W. Truran, and H. Tufo, Flash: An adaptive mesh hydrodynamics code for modeling astrophysical thermonuclear flashes, *ApJS* **131**, 273 (2000).

[36] A. Dubey, R. Fisher, C. Graziani, G. C. Jordan, IV, D. Q. Lamb, L. B. Reid, P. Rich, D. Sheeler, D. Townsley, and K. Weide, Challenges of Extreme Computing using the FLASH code, in *Numerical Modeling of Space Plasma Flows*, Astronomical Society of the Pacific Conference Series, Vol. 385, edited by N. V. Pogorelov, E. Audit, and G. P. Zank (2008) p. 145.

[37] L. M. Shivakumar and C. Federrath, Numerical viscosity and resistivity in MHD turbulence simulations, *Mon. Not. R. Astron. Soc.* **537**, 2961 (2025).

[38] V. Yakhot and D. A. Donzis, Emergence of multiscaling in a random-force stirred fluid, *Phys. Rev. Lett.* **119**, 044501 (2017).

[39] P. G. Huang, G. N. Coleman, and P. Bradshaw, Compressible turbulent channel flows: DNS results and modelling, *J. Fluid Mech.* **305**, 185–218 (1995).

[40] J. P. John, D. A. Donzis, and K. R. Sreenivasan, Solenoidal scaling laws for compressible mixing, *Phys. Rev. Lett.* **123**, 224501 (2019).

[41] S. Alam, D. Krasnov, A. Pandey, J. P. John, R. J. Samuel, P. P. Vieweg, and J. Schumacher, Turbulent mesoscale convection in the Boussinesq limit and beyond, *Int. J. Heat Fluid Flow* **115**, 109856 (2025).

[42] P. E. Hamlington, J. Schumacher, and W. J. A. Dahm, Local and non-local strain rate fields and vorticity alignment in turbulent flows, *Phys. Rev. E* **77**, 026303 (2008).

[43] D. A. Donzis and J. Panickacheril John, Universality and scaling in homogeneous compressible turbulence, *Phys. Rev. Fluids* **5**, 084609 (2020).

[44] C. Federrath, G. Chabrier, J. Schober, R. Banerjee, R. S. Klessen, and D. R. G. Schleicher, Mach number dependence of turbulent magnetic field amplification: Solenoidal versus compressive Flows, *Phys. Rev. Lett.* **107**, 114504 (2011).

[45] I. Staroselsky, V. Yakhot, S. Kida, and S. A. Orszag, Long-time, large-scale properties of a randomly stirred compressible fluid, *Phys. Rev. Lett.* **65**, 171 (1990).

[46] J. Wang, T. Gotoh, and T. Watanabe, Spectra and statistics in compressible isotropic turbulence, *Phys. Rev. Fluids* **2**, 013403 (2017).

[47] S. Jagannathan and D. A. Donzis, Reynolds and Mach number scaling in solenoidally-forced compressible turbulence using high-resolution direct numerical simulations, *J. Fluid Mech.* **789**, 669 (2016).

[48] V. Yakhot and K. R. Sreenivasan, Towards a dynamical theory of multifractals in turbulence, *Physica A* **343**, 147 (2004).

[49] G. Elsinga, T. Ishihara, and J. Hunt, Intermittency across reynolds numbers – the influence of large-scale shear layers on the scaling of the enstrophy and dissipation in homogenous isotropic turbulence, *J. Fluid Mech.* **974**, A17 (2023).

[50] D. A. Donzis, P. K. Yeung, and K. R. Sreenivasan, Dissipation and enstrophy in isotropic turbulence: Resolution effects and scaling in direct numerical simulations, *Phys. Fluids* **20**, 045108 (2008).

[51] P. K. Yeung, D. A. Donzis, and K. R. Sreenivasan, Dissipation, enstrophy and pressure statistics in turbulence simulations at high Reynolds numbers, *J. Fluid Mech.* **700**, 5 (2012).

Transition to dilatation-dominated compressible turbulence (Supplemental Material)

Shadab Alam¹, Christoph Federrath², and Jörg Schumacher¹

¹*Institut für Thermo- und Fluideodynamik, Technische Universität Ilmenau,*

Postfach 100565, D-98684 Ilmenau, Germany and

²*Research School of Astronomy and Astrophysics,
Australian National University, Canberra, ACT 2611, Australia*

(Dated: February 3, 2026)

DIRECT NUMERICAL SIMULATIONS

The compressible Navier-Stokes equations (2) and (3) of the main text are solved in a cube with volume $V = L^3$ and periodic boundary conditions in all three directions. We use a modified version of the FLASH code [1, 2], which is based on release 4.0.1 and employs the MUSCL-Hancock HLL5R scheme [3, 4]. The timestep is determined by the Courant-Friedrichs-Lowy (CFL) and diffusive stability conditions, whichever is more restrictive. The present version of FLASH [5, 6] is optimized for large-scale simulations using hybrid precision [7]: fluid variables are stored in single precision, while critical operations are performed in double precision. This approach preserves the accuracy of double-precision computations while reducing computational cost, communication overhead, and memory usage [6, 7]. The sound speed is kept constant at $c_s = 1$, while the mean kinetic energy injection rate $\langle \epsilon_{\text{in}} \rangle_{V,t} = \langle \rho \mathbf{f} \cdot \mathbf{u} \rangle_{V,t}$ is varied to attain the target M_t . For each fixed M_t , the Reynolds number is varied by adjusting ν .

Detailed simulation parameters, information about the resolution ($k_{\text{max}}\eta$), as well as maxima and minima of the normalized 4th-order moments of the total energy dissipation rate are listed in Tables I and II. We define $M_4 = \langle \epsilon^4 \rangle_{V,t} / \langle \epsilon \rangle_{V,t}^4$. Furthermore, we provide the number of statistically independent snapshots, N_s . Successive snapshots are separated by a quarter large-scale eddy-turnover time, $T_e/4$ with $T_e = L_f / u_{\text{rms}}$.

STATISTICAL CONVERGENCE OF DISSIPATION RATE MOMENTS

Figure 1 illustrates the convergence of the 4th-order moments of the total energy dissipation rate ϵ . We thus plot $\epsilon^4 p(\epsilon)$ versus ϵ for all Mach numbers M_t at the highest Reynolds number of $Re \approx 2400$. The panels show that all cases are converged, except for the data at $M_t = 0.55$. This series is characterized by a few extreme fluctuation events, which alter the overall statistics. Figure 2 displays the 4th-order moments obtained from the different snapshots at $M_t = 0.55$ and compares it with those at $M_t = 0.1$ and $M_t = 3$.

DECOMPOSITION OF KINETIC ENERGY DISSIPATION RATE

For completeness, we present the dissipation rate decomposition derived by Alam et al. [8]. The total kinetic energy dissipation rate field ϵ is expressed as

$$\epsilon(\mathbf{x}, t) = 2\mu S_{ij} S_{ij} - \frac{2\mu}{3} \left(\frac{\partial u_k}{\partial x_k} \right)^2. \quad (1)$$

The first term on the right-hand side of (1) can be expanded as follows,

$$2\mu S_{ij} S_{ij} = 2\mu \Omega_{ij} \Omega_{ij} + 2\mu \left[\frac{\partial u_i}{\partial x_j} \frac{\partial u_j}{\partial x_i} \right], \quad (2)$$

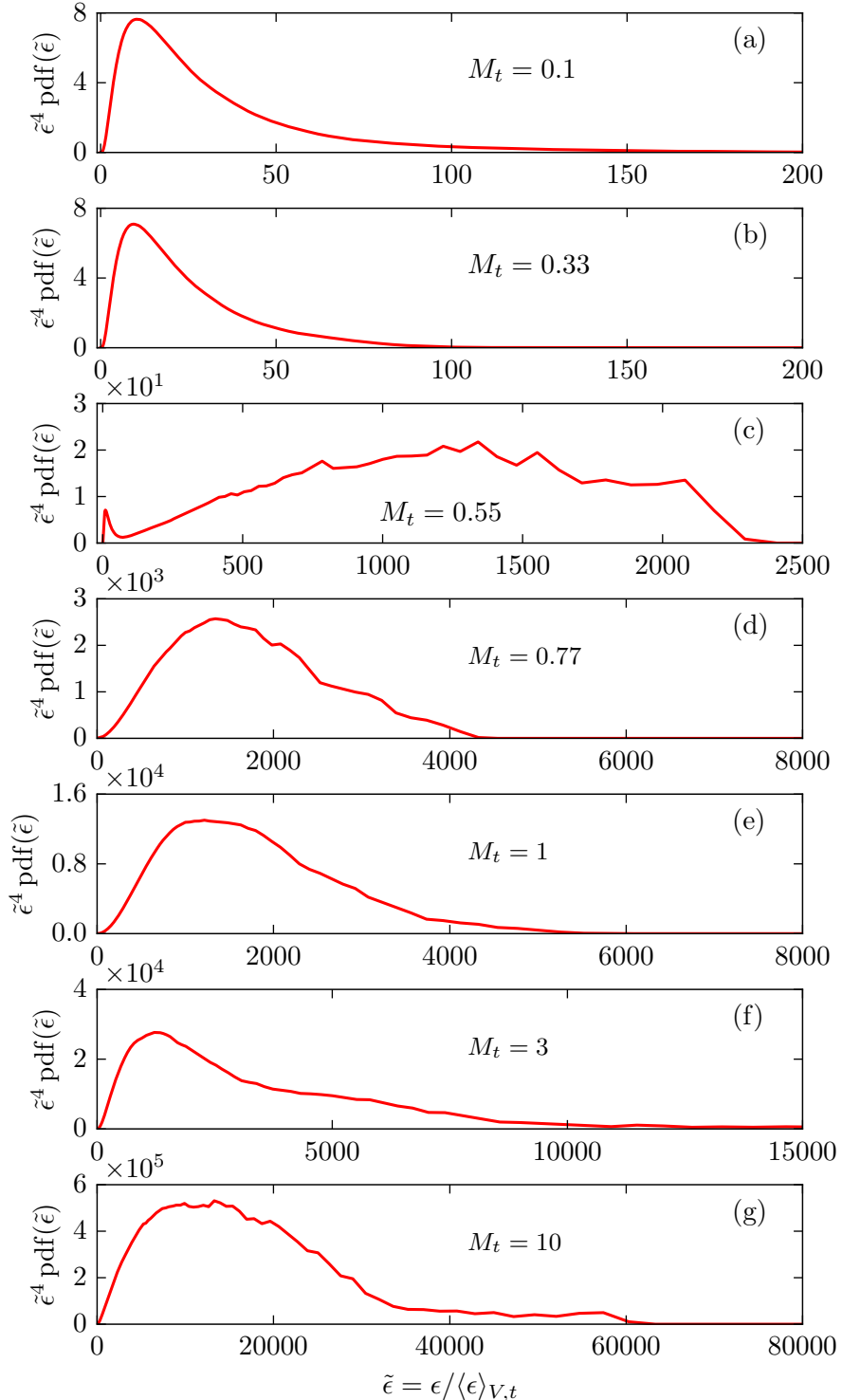


FIG. 1. Statistical convergence test of the normalized 4th-order moments of the total energy dissipation rate field for the highest Reynolds number runs ($Re \approx 2400$) at turbulent Mach numbers $M_t = 0.1$ (a), $M_t = 0.33$ (b), $M_t = 0.55$ (c), $M_t = 0.77$ (d), $M_t = 1$ (e), $M_t = 3$ (f), $M_t = 10$ (g).

Run	N^3	M_t	Re	Re_λ	N_s	M_4	$\min[M_4]$	$\max[M_4]$	$k_{\max}\eta$
1	512^3	0.10	100	17	100	1.67×10^1	6.24×10^0	4.06×10^1	29.14
2	512^3	0.10	219	29	100	2.92×10^1	6.24×10^0	1.02×10^2	17.44
3	512^3	0.10	399	43	100	4.31×10^1	1.01×10^1	1.10×10^2	11.57
4	1024^3	0.10	520	50	100	5.65×10^1	2.00×10^1	1.52×10^2	19.24
5	1024^3	0.10	709	58	100	7.12×10^1	1.19×10^1	2.01×10^2	15.26
6	1024^3	0.10	932	67	100	1.01×10^2	1.39×10^1	6.14×10^2	12.40
7	2048^3	0.10	2469	117	100	2.67×10^2	4.76×10^1	1.08×10^3	12.40
8	512^3	0.34	102	17	100	1.78×10^1	5.30×10^0	5.70×10^1	29.12
9	512^3	0.33	222	29	100	2.78×10^1	8.10×10^0	1.02×10^2	17.28
10	512^3	0.33	391	42	100	4.49×10^1	1.18×10^1	1.45×10^2	11.73
11	1024^3	0.33	511	49	100	6.36×10^1	1.36×10^1	4.64×10^2	19.46
12	1024^3	0.33	715	59	100	7.16×10^1	2.25×10^1	2.70×10^2	15.24
13	1024^3	0.33	956	70	100	1.03×10^2	1.74×10^1	1.17×10^3	12.38
14	2048^3	0.33	2411	116	100	1.99×10^2	5.50×10^1	8.10×10^2	12.63
15	512^3	0.55	96	16	200	1.93×10^1	4.85×10^0	5.55×10^1	29.87
16	512^3	0.54	213	30	200	3.02×10^1	7.12×10^0	1.65×10^2	18.33
17	512^3	0.54	378	41	200	6.66×10^1	7.21×10^0	1.18×10^3	12.04
18	1024^3	0.55	497	48	200	3.94×10^2	1.57×10^1	6.16×10^4	19.75
19	1024^3	0.56	712	61	100	8.24×10^3	2.47×10^1	8.02×10^5	15.51
20	1024^3	0.56	955	71	100	1.71×10^4	2.87×10^1	1.12×10^6	12.46
21	2048^3	0.56	2405	114	100	2.31×10^4	3.30×10^1	8.85×10^5	12.59
22	512^3	0.78	97	17	200	7.39×10^1	4.98×10^0	4.27×10^3	29.55
23	512^3	0.77	212	29	200	5.03×10^2	6.99×10^0	2.41×10^4	17.90
24	512^3	0.77	385	42	200	1.94×10^4	1.46×10^1	1.04×10^6	11.91
25	1024^3	0.78	505	49	200	7.48×10^4	6.11×10^1	4.12×10^6	19.67
26	1024^3	0.77	695	59	100	1.05×10^5	3.52×10^2	2.06×10^6	15.68
27	1024^3	0.78	947	70	100	2.22×10^5	2.37×10^3	2.16×10^6	12.50
28	2048^3	0.78	2414	116	100	3.61×10^6	4.68×10^4	3.36×10^7	12.60
29	512^3	1.0	95	16	200	2.34×10^2	7.03×10^0	4.41×10^3	29.60
30	512^3	1.0	218	29	200	6.54×10^3	2.95×10^1	1.22×10^5	17.41
31	512^3	1.0	386	42	200	7.14×10^4	4.10×10^2	1.50×10^6	11.88
32	1024^3	1.0	499	49	200	2.17×10^5	1.49×10^3	2.57×10^6	19.77
33	1024^3	1.0	686	58	100	7.02×10^5	7.44×10^3	1.01×10^7	15.71
34	1024^3	1.0	927	68	100	1.22×10^6	2.78×10^4	1.14×10^7	12.62
35	2048^3	1.0	2389	114	100	1.29×10^7	1.52×10^6	4.94×10^7	12.66

TABLE I. Direct numerical simulation (DNS) parameters of solenoidally forced compressible isotropic turbulence. The Run number, turbulent Mach number M_t , large-scale Reynolds number Re , Taylor micro-scale Reynolds number Re_λ , statistically independent snapshots N_s , minima and maxima of M_4 , and $k_{\max}\eta$.

where $\Omega_{ij} = (\partial u_i / \partial x_j - \partial u_j / \partial x_i) / 2$ is the anti-symmetric vorticity tensor and $S_{ij}\Omega_{ij} = 0$. Using the product rule, we express the second term on the right hand side of (2) as

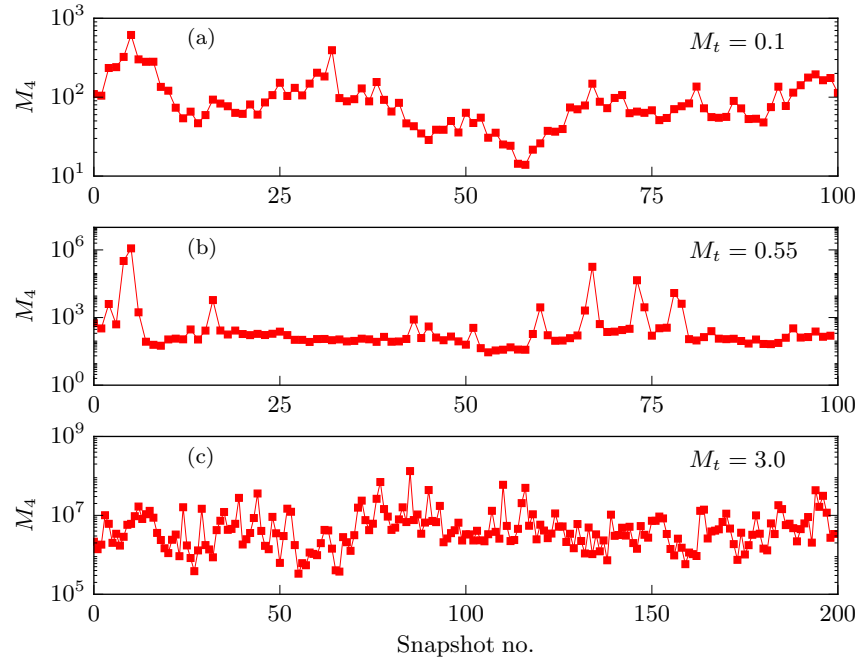
$$\begin{aligned}
2\mu \left[\frac{\partial u_i}{\partial x_j} \frac{\partial u_j}{\partial x_i} \right] &= 2\mu \left[\frac{\partial}{\partial x_j} \left\{ u_i \frac{\partial u_j}{\partial x_i} \right\} - u_i \frac{\partial}{\partial x_j} \left(\frac{\partial u_j}{\partial x_i} \right) \right] \\
&= 2\mu \frac{\partial}{\partial x_j} \left\{ \frac{\partial}{\partial x_i} (u_i u_j) - u_j \frac{\partial u_i}{\partial x_i} \right\} - 2\mu \left\{ \frac{\partial}{\partial x_i} \left(u_i \frac{\partial u_j}{\partial x_j} \right) - \left(\frac{\partial u_j}{\partial x_j} \right)^2 \right\} \\
&= 2\mu \frac{\partial^2}{\partial x_i \partial x_j} (u_i u_j) - 4\mu \frac{\partial}{\partial x_i} \left(u_i \frac{\partial u_k}{\partial x_k} \right) + 2\mu \left(\frac{\partial u_k}{\partial x_k} \right)^2. \tag{3}
\end{aligned}$$

Combining eqns. (1), (2), and (3) yields the decomposition,

$$\epsilon = \epsilon_s + \epsilon_d + \epsilon_I, \tag{4}$$

Run	N^3	M_t	Re	Re_λ	N_s	M_4	$\min[M_4]$	$\max[M_4]$	$k_{\max}\eta$
36	512^3	3.0	95	15	200	2.75×10^4	1.61×10^2	9.91×10^5	28.31
37	512^3	3.0	217	25	200	1.62×10^5	5.15×10^3	3.82×10^6	16.21
38	512^3	3.1	390	35	200	7.62×10^5	1.44×10^4	1.22×10^7	11.72
39	1024^3	3.0	507	40	200	4.29×10^6	4.93×10^4	1.26×10^8	17.65
40	1024^3	3.0	721	50	200	5.23×10^6	9.73×10^4	1.21×10^8	13.88
41	1024^3	3.1	944	56	200	7.41×10^6	3.33×10^5	1.33×10^8	11.27
42	2048^3	3.0	2360	95	132	1.10×10^8	5.24×10^6	1.16×10^9	11.68
43	512^3	6.2	104	16	200	9.86×10^5	2.50×10^3	9.34×10^7	26.93
44	512^3	6.2	207	24	200	3.57×10^6	6.77×10^3	2.27×10^8	16.75
45	512^3	6.2	416	36	200	2.07×10^8	1.69×10^5	3.72×10^{10}	10.19
46	1024^3	6.2	519	40	200	1.03×10^8	3.79×10^5	5.52×10^9	17.33
47	1024^3	6.2	724	48	200	1.29×10^8	8.48×10^5	5.58×10^9	13.62
48	1024^3	6.2	1034	58	200	7.41×10^6	8.59×10^5	2.22×10^{10}	11.01
49	2048^3	6.3	2631	96	150	1.10×10^8	1.92×10^7	1.73×10^{12}	11.02
50	512^3	10.2	98	15	200	2.04×10^6	4.36×10^3	9.36×10^7	28.41
51	512^3	10.2	222	25	200	7.54×10^7	1.38×10^5	6.60×10^9	15.99
52	512^3	10.3	396	35	200	1.06×10^8	7.20×10^5	2.50×10^9	11.64
53	1024^3	10.2	510	40	200	4.48×10^8	2.27×10^6	1.26×10^{10}	17.54
54	1024^3	10.2	714	48	200	1.05×10^9	2.32×10^6	3.28×10^{10}	13.67
55	1024^3	10.3	958	56	200	5.48×10^9	6.30×10^6	3.89×10^{11}	11.06
56	2048^3	10.4	2445	92	146	2.28×10^{10}	1.00×10^8	1.48×10^{12}	11.10

TABLE II. Continued from Table I.

FIG. 2. 4th-order moments of the total dissipation rate at turbulent Mach numbers $M_t = 0.1$ (a), $M_t = 0.55$ (b), and $M_t = 3.0$ (c).

with the solenoidal (s), dilatational (d), and inhomogeneous (I) components, which follow to

$$\epsilon_s(\mathbf{x}, t) = 2\mu\Omega_{ij}\Omega_{ij}, \quad \epsilon_d(\mathbf{x}, t) = \frac{4\mu}{3} \left(\frac{\partial u_k}{\partial x_k} \right)^2, \quad \epsilon_I(\mathbf{x}, t) = 2\mu \left[\frac{\partial^2}{\partial x_i \partial x_j} (u_i u_j) - 2 \frac{\partial}{\partial x_i} \left(u_i \frac{\partial u_k}{\partial x_k} \right) \right]. \quad (5)$$

Using the definition of vorticity vector field $\omega_i = -\varepsilon_{ijk}\Omega_{jk}$, where ε_{ijk} is the Levi-Civita symbol, it can be shown that the local enstrophy $\mathcal{E} = \omega_i \omega_i = 2\Omega_{jk}\Omega_{jk} = (\nabla \times \mathbf{u})^2$. Thus, $\epsilon_s = 2\mu\Omega_{ij}\Omega_{ij} = \mu\mathcal{E}$. For constant viscosity μ , the

n	$\tilde{\beta}_{\text{ens},n}$	$\beta_{\text{ens},n}$
2	0.21	0.23
3	0.42	0.70
4	0.57	1.27

TABLE III. Scaling exponents of enstrophy moments in incompressible homogeneous isotropic turbulence, as reported in a DNS study [9].

solenoidal dissipation rate ϵ_s is then directly proportional to the local enstrophy, \mathcal{E} . In vector notation, the dissipation components read

$$\epsilon_s(\mathbf{x}, t) = \mu(\nabla \times \mathbf{u})^2, \quad \epsilon_d(\mathbf{x}, t) = \frac{4}{3}\mu(\nabla \cdot \mathbf{u})^2, \quad \epsilon_I(\mathbf{x}, t) = 2\mu [(\nabla \otimes \nabla) : (\mathbf{u} \otimes \mathbf{u}) - 2\nabla \cdot (\mathbf{u}(\nabla \cdot \mathbf{u}))].$$

This is given in the main text.

SCALING EXPONENTS OF ENSTROPY MOMENTS

For incompressible turbulence, Elsinga *et al.* [9] investigated the anomalous scaling of enstrophy moments with respect to the Taylor microscale Reynolds number Re_λ . In their analysis, the scaling was characterized using the n th-order moment raised to the power $1/n$, defined as

$$\tilde{M}_{\text{ens},n} = \frac{\langle \mathcal{E}^n \rangle_{V,t}^{1/n}}{\langle \mathcal{E} \rangle_{V,t}^n} \sim Re_\lambda^{\tilde{\beta}_{\text{ens},n}}. \quad (6)$$

This definition can be expressed with respect to the large-scale Reynolds number Re and written directly in terms of the normalized n th-order moment, without taking the $1/n$, i.e.,

$$M_{\text{ens},n} = \frac{\langle \mathcal{E}^n \rangle_{V,t}}{\langle \mathcal{E} \rangle_{V,t}^n} \sim Re^{\beta_{\text{ens},n}} \quad \text{where} \quad \beta_{\text{ens},n} = \frac{n \tilde{\beta}_{\text{ens},n}}{C}. \quad (7)$$

Here, we have used the relation $Re \sim Re_\lambda^C$ reported by Elsinga *et al.* [9], based on a fit to the DNS data of Schumacher *et al.* [10] with the fit coefficient $C = 1.8$. The resulting scaling exponents are listed in Table III. In the incompressible limit ($M_t \ll 1$), the dynamic viscosity $\mu = \rho\nu$ is constant, and the solenoidal dissipation component ϵ_s is therefore directly proportional to the local enstrophy. Consequently, the scaling exponents of the moments of ϵ_s coincide with the enstrophy exponents, i.e. $\beta_{s,n} \approx \beta_{\text{ens},n}$, see again Fig. 3(b) in the main text.

- [1] B. Fryxell, K. Olson, P. Ricker, F. X. Timmes, M. Zingale, D. Q. Lamb, P. MacNeice, R. Rosner, J. W. Truran, and H. Tufo, *ApJS* **131**, 273 (2000).
- [2] A. Dubey, R. Fisher, C. Graziani, G. C. Jordan, IV, D. Q. Lamb, L. B. Reid, P. Rich, D. Sheeler, D. Townsley, and K. Weide, in *Numerical Modeling of Space Plasma Flows*, Astronomical Society of the Pacific Conference Series, Vol. 385, edited by N. V. Pogorelov, E. Audit, and G. P. Zank (2008) p. 145.
- [3] F. Bouchut, C. Klingenber, and K. Waagan, *Numer. Math.* **115**, 647–679 (2010).
- [4] K. Waagan, C. Federrath, and C. Klingenber, *J. Comput. Phys.* **230**, 3331 (2011).
- [5] S. Cielo, L. Iapichino, J. Günther, C. Federrath, E. Mayer, and M. Wiedemann, *Parallel Comput.* **102**, 102758 (2021).
- [6] C. Federrath, R. S. Klessen, L. Iapichino, and J. R. Beattie, *Nat. Astron.* **5**, 365 (2021).
- [7] C. Federrath and S. Offner, *Living Rev. Comput. Astrophys.* , arXiv:2510.12203 (2025).
- [8] S. Alam, D. Krasnov, A. Pandey, J. P. John, R. J. Samuel, P. P. Vieweg, and J. Schumacher, *Int. J. Heat Fluid Flow* **115**, 109856 (2025).
- [9] G. Elsinga, T. Ishihara, and J. Hunt, *J. Fluid Mech.* **974**, A17 (2023).
- [10] J. Schumacher, K. R. Sreenivasan, and V. Yakhot, *New. J. Phys.* **9**, 89 (2007).